THE JOURNAL OF PHYSICAL CHEMISTRY B

Article

pubs.acs.org/JPCB

Poly(vinyl alcohol) Oligomer in Dilute Aqueous Solution: A Comparative Molecular Dynamics Simulation Study

Giulio Tesei, Gaio Paradossi, and Ester Chiessi*

Department of Chemical Sciences and Technologies, University of Rome, Tor Vergata, Via della Ricerca Scientifica I, 00133 Rome, Italy

Supporting Information

ABSTRACT: Molecular dynamics (MD) simulations of a poly(vinyl alcohol), PVA, oligomer in very diluted aqueous solution have been carried out, at the 2-fold aim to investigate structural and dynamical features of this system and to comparatively test the robustness of G45A3 and G45A4 GROMOS force fields in modeling PVA in aqueous environment. An atactic PVA chain of 30 repeating units in water at concentration of 3% (w/w) has been simulated at 293, 303, and 323 K. The trajectory analysis has focused on the temperature influence on chain size, conformational properties and intramolecular hydrogen bonding of PVA. The PVA−water interaction and the polymer induced modifications of water properties have been also investigated. Simulation results have been compared with available experimental data on PVA aqueous solutions, in order to evaluate the reliability of these force fields in the MD simulation of PVA-based systems in aqueous environment. Findings obtained from the simulations with the G45A4 force field have shown a better agreement with experimental results and have highlighted peculiar structural and dynamical characteristics of PVA in dilute aqueous solution. In particular, the simulation has shown a heterogeneity in the overall chain structure, not affected by temperature, and the absence of intrachain hydrogen bonds between nonadjacent residues. The trajectory analysis has revealed that the polymer influence on water structure and dynamics involves about six water molecules per PVA residue.

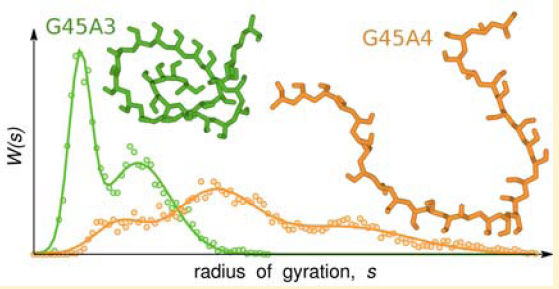

1. INTRODUCTION

Poly(vinyl alcohol) (PVA) is an ancient synthetic macromolecule[1] that finds several applications in modern technology, ranging from membrane-based liquid and gas mixtures separation[2−5] to composite reinforcement and encapsulation of bacteria by electrospinning techniques.[6,7] Because of the action of many microorganisms, belonging to Pseudomonas, Alcaligenes, and Bacillus genuses,[8] this macromolecule is perhaps the only biodegradable vinyl homopolymer,[9,10] a relevant property for its green disposal.

In the last 3 decades, PVA has become popular as soft biomaterial, due to nontoxicity,[11,12] hydrophilicity, and possibility to be functionalized according to the requirements of the final biomedical device. A large amount of studies about chemically[13−16] and physically[17] cross-linked PVA-based hydrogels and microgels for controlled drug delivery is reported in the literature. Devices with advanced functionalities, such as targeting of specific tissues and diagnostic enhancing ability, have been designed and developed.[18−20] Typically, these systems are highly hydrated polymer networks, with pore sizes of a few nanometer, where the PVA behavior affects the properties of loading/release of drugs, the transport of metabolites, the overall rheology of the matrix and the mechanisms of physical processes which are relevant for use.

In a large class of PVA-based hydrogels the junctions between chains are formed by covalent bonds between suitable chemical groups of functionalized PVAs. When the fraction of modified PVA residues is limited and consequently the degree of cross-linking of the network is low, the properties of these hydrogels are strictly related to the behavior of the polymer in solution. The other class of PVA hydrogels includes the physically cross-linked networks, where the junctions are crystallite domains formed by freezing/thawing cycles on the PVA aqueous solution.[21−24] In the latter systems, the polymer−water interaction and the local chain dynamics are similar to those of PVA in solution, with the exclusion of the junction domains. For these reasons, the understanding of the polymer properties in homogeneous aqueous solution is valuable for designing hydrogel matrices with specific characteristics for applications in a high hydration regime.

However, it is noteworthy that the temperature effect on the PVA chain behavior in aqueous solution is particularly complex and not yet completely understood.[25,26] Experimental studies suggest the presence of superstructured domains in the PVA chain in water[27−29] and show a phase behavior based on a delicate balance of hydrophilic/hydrophobic interactions.[30] Moreover, the amount of water strongly interacting with PVA in dilute solution, with values ranging from 2 up to 7 water

Received: May 31, 2012
Revised: July 20, 2012
Published: July 27, 2012

molecules per PVA residue, depending on the experimental method,[31−33] is still a matter of debate.

The motivation of the present study is to contribute to elucidate the PVA behavior in dilute aqueous solution by means of molecular dynamics simulation (MD), in the perspective to use this information for the characterization of PVA hydrogels at high hydration degree.

The MD simulation method was recently applied by us to investigate the temperature induced transition of poly(*N*-isopropylacrylamide) in water[34,35] and to characterize structural and dynamic properties of polymer hydrogels in a nanoscale domain, providing an atom detailed picture to compare with experimental findings.[36,37] A number of simulation studies on PVA in aqueous environment is reported in the literature. This work developed in phases, following the increase of performance of the simulation tools. In 1983, one of the first computing studies on PVA tackled the problem of the conformational features, without explicitly accounting for the solvent.[38] Then, at the end of the nineties, the MD studies of Tamai et al. described the structure and dynamics of water in systems containing a PVA oligomer, with degree of polymerization from 21 to 161 repeating units, in the presence of hundreds of water molecules. An AMBER/OPLS force field with united atom treatment of the CH_n groups and the SPC/E and TIP4P models were used for PVA and water, respectively. The production runs covered time intervals from tens to a few thousand picoseconds.[39−45] In the same years Müller-Plathe reported MD investigations of a 15-mer and a 400-mer in water.[46−48] For the longest PVA chain the effect of the polymer on the solvent behavior as a function of hydration, ranging from about 10 to 40% (w/w) of water, was studied.[48] In these works an all-atom force field, derived from ethanol and poly(ethylene oxide) simulations, and the SPC model were used for PVA and water, respectively, and the explored trajectory intervals covered about 10 ns.[46−48] A few year later Hedenqvist et al. published the studies of an atactic 145-mer[49] and a syndiotactic 600-mer,[50] focusing on water and oxygen diffusivity in these materials. They applied a PVA adapted all-atom AMBER force field, with production runs of about 10 ns. Two recent MD simulation works on PVA investigated a single chain of 300 residues in water.[51,52] Bermejo at al. described the polymer structure and mobility as a function of water content, ranging from 10 to 80% (w/w), using the all-atom COMPASS force field and with production runs over 10−20 ns.[51] Wu reported about the cooperative behavior of poly(vinyl alcohol) and water, simulating a 300-mer in the presence of 200 water molecules with a hybrid OPLS-AA/COMPASS force field and TIP4P water model, in 10 ns production runs.[52] In addition to the classical MD simulation works, an ab initio MD study of a five residue isotactic PVA fragment in the presence of 75 water molecules was recently reported.[53]

This literature summary shows that the progression of MD simulation studies of PVA in water followed the performances of computing facilities in terms of explored space and time windows, thus arriving to model a single chain of a few hundred of residues at a 80% (w/w) maximum hydration degree for about 20 ns.

In the present study we exploit the current computing capabilities to investigate the solution behavior of PVA in an almost infinite dilution regime, where the polymer structure and dynamics are dictated only by intramolecular interactions and by the solvent environment. This choice derives from (a) the necessity to separately evaluate the elements determining the polymer properties in water, excluding interchain effects; (b) the availability of recent experimental results on PVA solution at low concentration and on PVA single chain in water; (c) the need to model a system with a very high water content, similar to that where PVA hydrogels for biomedical applications usually work. Here we model a PVA 30-mer in water, at a concentration of 3% (w/w) in a temperature range from 293 to 323 K, including the physiological condition. At our best knowledge, this is the first MD simulation study of an atactic PVA oligomer at such a low concentration.

The objective of this work is 2-fold. First, to clarify the complex behavior of PVA in water as a function of temperature, both in the aspects concerning the chain size and in those involving the intramolecular connectivity. Second, to validate an MD simulation approach to apply in the study of more complex PVA-based systems, such as highly hydrated polymer networks. For the second aim, we decided to carry out a comparative simulation of two force field conditions and to devote a particular attention to the equilibration requirements. The force fields here tested offer the advantage of accessibility, being implemented by the free and highly performing software package GROMACS. For the first and second aim, we perform a strict comparison of the simulation results with available experimental findings, both to enrich the experimental data with an atomic detailed interpretation of PVA structural and dynamical features in water and to select the best protocol on a justified basis.

2. COMPUTING DETAILS

Developing a MD simulation protocol suitable to model PVA-based hydrogels and easily implementable is one of the motivations of this study. A realistic modeling of a hydrated polymer network has to include a representative domain of the system, covering a typical volume of 10^3 nm^3, and to explore time windows of several tens of nanoseconds for a reliable evaluation of properties. For these reasons, we worked within the free GROMACS software environment (version 4.5.5),[54−56] which provides a highly performing MD simulation engine, and we selected force fields using the CH_n united atom convention, allowing a larger size of the polymer model for the same computing cost.

Using the same starting system configuration, we carried out two parallel simulation routes, identical in the procedure but differing in the force field (FF). For one simulation series, hereafter named as A3 simulation, we used the GROMOS 45A3 FF, an evolution of the FF for biomolecular systems GROMOS96 45A1, aimed to model aliphatic hydrocarbons in the condensed phase.[57,58] For the other simulation series, hereafter named as A4 simulation, we used the GROMOS 45A4 FF, where some modifications to the 45A3 FF were specifically carried out to model carbohydrate molecules.[59] The GROMOS 45A4 FF also provides a new parametrization of the atomic partial charges of ethanol, that improves the simulation of the aqueous solvation properties of this molecule.[59] Taking into account that ethanol is the molecule corresponding to the repeating unit of PVA, in the A4 simulation we chose to test the 45A4 ethanol model for modeling the atomic partial charges of PVA residues.

Both GROMOS 45A3 and 45A4 FFs use the united atom convention for CH, CH_2 and CH_3 groups and they are refined for the single-point charged (SPC) intermolecular potential water model.[60] Therefore, the difference between A3 and A4 simulations concerns only the values of the atomic partial

charges of polymer atoms (shown in Table 1), all other FF parameters and conditions remaining the same.

Table 1. Comparison between Partial Charges Parametrization of PVA in A3 and A4 Simulations

	A3		A4	
atom type	charge [e]	charge group	charge [e]	charge group
CH2 or CH3	0.000	0	0.000	0
CH	0.150	1	0.232	0
OA	−0.548	1	−0.642	0
H	0.398	1	0.410	0

A PVA oligomer of 30 repeating units (Chart 1) was generated in all-trans conformation with a molecular builder

Chart 1. Nomenclature of PVA Oligomer, n = 29

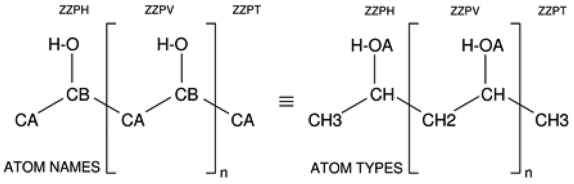

program of the CHARMM software package,[61] starting from the internal coordinates of the residue. An atactic chain was obtained by fixing the improper dihedral terms of −CHOH- groups in a randomly generated sequence of d and l configurations. The ratio between the number of meso (m) and racemo (r) dyads, m/r, of the oligomer was 16/13. After minimization of energy, a 0.5 ns MD simulation trajctory in vacuo at 313 K was acquired (time step 0.5 fs). In this initial phase the GROMOS 45A3 FF was used. From the trajectory in vacuo we selected a structure where the end-to-end distance, r, of the oligomer was in agreement with eq 1

$$\langle r^2 \rangle = nl^2 C_\infty \tag{1}$$

where C_∞ is the characteristic ratio of PVA in water, equal to 8.3 at 30 °C,[62] n is the number of C−C bonds of the oligomer and l is the C−C bond distance. This structure was inserted in a cubic box with 3.4 nm side and hydrated with 2412 water molecules, for a resulting PVA concentration of 3% (w/w).

Thereafter, the simulation work was split up into the A3 and A4 parallel procedures, using the GROMOS 45A3 and GROMOS 45A4 FF's, respectively. The hydrated 30-mer configuration was energy minimized, using the steepest descent algorithm with a tolerance of 30 kJ·mol^{-1}·nm^{-1}, and MD simulation trajectories in the NPT ensemble were acquired for about 30 ns at 293, 303, and 323 K, at the aim to equilibrate the system. At the end of the NPT runs the box side was about 4.1 nm. The leapfrog integration algorithm[63] with a 2-fs time step, cubic periodic boundary conditions and minimum image convention were used. The LINCS procedure[64] was applied to constrain all bond lengths. Temperature was controlled with the Berendsen's coupling algorithm,[65] with a time constant of 0.1 ps. The pressure was maintained at 1.0 bar by a Berendsen isotropic coupling,[65] with a relaxation time of 0.5 ps. Electrostatic interactions were calculated by the smooth particle-mesh Ewald method,[66] the cutoff of nonbonded interactions being set to 1.4 nm. The last configuration of the NPT runs at each temperature was used in subsequent MD simulations performed in the NVT ensemble for further 50 ns. The 20−50 ns trajectory interval of the *NVT* runs was considered for analysis. In the production runs temperature was controlled using the velocity rescaling thermostat coupling algorithm[67] over two groups (PVA and water) and a time constant of 0.1 ps. The configurations were saved every 5 ps.

The total simulation time, including equilibration, was about 90 ns for each temperature, for both A3 and A4 simulations.

The system equilibration was carefully monitored. During the NPT runs density, energy and temperature were equilibrated to final drift/ns lower than 0.006%. The equilibration of the polymer component was checked by following the time behavior of the root mean squared deviation of all N polymer atoms, rmsd:

$$\mathrm{rmsd}(t + t_0) = \left[\frac{1}{M} \sum_{i=1}^{N} m_i \| r_i(t + t_0) - r_i(t_0) \|^2 \right]^{1/2} \tag{2}$$

The reference structure is the starting polymer configuration (t_0 = 0) of the *NPT* run. The rmsd was calculated after roto-translational fit on the PVA backbone atoms. In the last 30 ns of the *NVT* runs, considered for analysis, the rmsd displayed an oscillating behavior with a drift/ns lower than 1.1% of the rmsd average value.

A specific sampling of the trajectory was carried out for investigating polymer−water interaction and water properties. Three values of time (t_1, t_2, t_3), 10 ns apart, were selected within the 30 ns production runs. Starting from t_1, t_2, t_3, the system configurations were saved every 0.1 ps for the subsequent 0.5 ns. These most frequently sampled trajectory portions were used for the analysis of properties directly involving water, whose values were obtained as averages over the three 0.5 ns trajectories. We checked that this sampling procedure was meaningful by verifying the agreement between the average radial distribution function between PVA and water oxygen atoms, $g_{O\text{-}OW}(r)$, obtained from the frequently sampled trajectory intervals and the same function calculated over the whole 30 ns production run.

Corresponding MD simulations of a water box with the same size of the PVA solution, containing 2483 molecules, were carried out to obtain the bulk water properties for a comparison. For each temperature a trajectory of 0.5 ns was calculated.

The computing activity was performed on the IBM-SP6 Cluster of 168 Power6 575 nodes at the CINECA Supercomputing Center (Bologna, Italy).

In the following of this section, we report some information about the procedures used for the trajectory analysis.

The distribution of the radius of gyration of the PVA oligomer, s, was analyzed by fitting data to bimodal or trimodal normal distributions, according to eq 3

$$W(s) = \sum_{j=1}^{L} \frac{w_j}{\sqrt{2\pi\sigma_j}} e^{-(s-s_{0,j})^2/2\sigma_j} \tag{3}$$

where $W(s)$ is the normalized distribution function of s values, calculated with a bin of 0.01 nm, and L is set equal to 2 or 3, for bimodal or trimodal distributions, respectively.

The hydrogen bonding (HB) was studied by analyzing the trajectory for the occurrence of this interaction, adopting as geometric criteria an acceptor−donor distance (A···D) lower than 0.35 nm and an angle Θ (A···D-H) lower than 30°.

The HB between PVA residues (intramolecular HB) was analyzed even using the definition of a hydrogen-acceptor

dx.doi.org/10.1021/jp305296p | J. Phys. Chem. B 2012, 116, 10008−10019

distance (H···A) lower than 0.245 nm and $\Theta < 30°$. The value of 0.245 nm is the first minimum distance of the radial distribution function between the hydrogen and oxygen atoms of PVA, $g_{H-O}(r)$. The differences between the results obtained with the two HB definitions were within errors.

In the analysis of intramolecular HB we distinguished the contribution of HB between near-neighboring PVA residues, at the aim to assess the average fraction of PVA residues involved in HB with adjacent residues, $\langle f_a \rangle$. The value of $\langle f_a \rangle$ for PVA in aqueous solution, experimentally estimated by means of CP/MAS ^{13}C NMR measurements, provides a comparison element for our simulations.[68] For each frame we calculated the number of HBs formed between the i-th and $(i + 1)$th PVA residues, $n_{HB,i-(i+1)}$, and we analyzed the formation of sequential HBs between adjacent OH groups of PVA. Sequences of two or more PVA adjacent residues mutually connected by HBs were found (Figure 1). The average length (in residues) of these

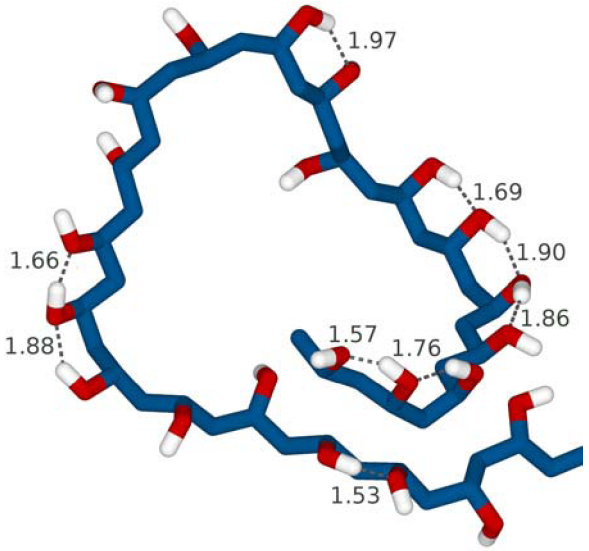

Figure 1. Sequences of PVA residues connected by intradyad HBs. Four, three, and two residues sequences are shown, from a trajectory snapshot of the A4 simulation at 303 K. Distances between oxygen and hydrogen atoms involved in HB are reported in Å.

sequences, μ, was calculated for each frame and f_a was then obtained by eq 4

$$f_a(t) = \frac{n_{HB,i-(i+1)}(t)}{N} \times \frac{\mu(t)}{\mu(t) - 1} \tag{4}$$

where N is the total number of PVA residues. The value of $\langle f_a \rangle$ was finally obtained by time averaging over the production run.

HB between PVA and water was analyzed in the most frequently sampled trajectory segments.

The HB dynamics was evaluated by studying the normalized time autocorrelation function $C_{HB}(t)$

$$C_{HB}(t) = \frac{\langle s_{ij}(t_0) s_{ij}(t + t_0) \rangle}{\langle s_{ij}(t_0) s_{ij}(t_0) \rangle} \tag{5}$$

where the state variable s_{ij} has a value of 1 or 0 depending on the existence or nonexistence of an HB between a selected donor−acceptor pair ij. t_0 and t in eq 5 range from 0 to half of the simulation time considered for analysis. The function $s_{ij}(t + t_0)$ is set to 1 if the HB between ij is found to be present in the time steps t_0 and $t_0 + t$, even if the same HB can be interrupted in some intermediate time. This definition of $C_{HB}(t)$ corresponds to the intermittent HB autocorrelation function, described by Rapaport[69] and Luzar,[70] where the correlation of a particular donor−acceptor pair is evaluated irrespective of possible prior bond breaking and reforming events. With this choice the correlation time, τ_{HB}, estimates the average lifetime of interaction for the ensemble of HB pairs, within the time window of the analyzed trajectory time. The correlation time, τ_{HB}, was obtained by integration of $C_{HB}(t)$ in a time window where the decay of the function was greater than 99%.

Water diffusion coefficient, D_W, was obtained from the long-time slope of the mean squared displacement, eq 6

$$D_W = \frac{1}{6} \lim_{t \to \infty} \frac{d}{dt} \langle |\mathbf{r}(t) - \mathbf{r}(0)|^2 \rangle \tag{6}$$

where $\mathbf{r}(t)$ and $\mathbf{r}(0)$ correspond to the position vector of the water oxygen at time t and 0, respectively, with an average performed over both time origins and water molecules. The ensemble of water molecules residing at a distance lower than 0.6 nm from PVA at t_0 and remaining in this environment during the following 10 ps trajectory interval was selected. This time-window corresponds to the characteristic time of the polymer−solvent interaction, as estimated by the average lifetime of hydrogen bond between PVA hydroxyl groups and water. The mean squared displacement of these selected water molecules was calculated during the $(t_0 + 10)$ ps trajectory and the diffusion coefficient value was obtained from the slope of the mean squared displacement vs time in the second half of the explored time window, when the double log plot of the mean squared displacement vs time displayed a linear behavior with a slope of 1. At the aim to improve the statistics the D_W analysis was performed every 0.01 ns over the most frequently sampled trajectory segments.

The graphic visualization was done using the molecular viewer software package VMD.[71]

3. RESULTS AND DISCUSSION

3.1. PVA Properties. The overall chain behavior of the PVA oligomer was analyzed by means of the radius of gyration, s, and the end to end distance, r, both properties monitoring the oligomer extension in solution. Figure 2 shows the trajectory of s at 293, 303, and 323 K, by comparing the

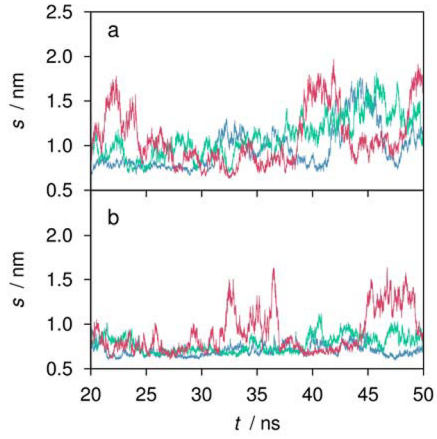

Figure 2. Trajectory of the radius of gyration at 293 K (blue), 303 K (green) and 323 K (red), in A4 (a) and A3 (b) simulations.

dx.doi.org/10.1021/jp305296p | J. Phys. Chem. B 2012, 116, 10008−10019

Table 2. Overall Chain Properties

	A3			A4		
	T = 293 K	T = 303 K	T = 323 K	T = 293 K	T = 303 K	T = 323 K
$\langle r \rangle$ (nm)[a]	1.2(2)	1.2(1)	1.6(5)	1.7(1)	1.9(1)	1.8(1)
$\langle s \rangle$ (nm)[a]	0.71(2)	0.78(4)	0.9(1)	1.0(1)	1.1(2)	1.1(1)
s_{01} (nm)[b]	0.688(8)	0.710(2)	0.730(6)	0.797(4)	0.80(2)	0.84(4)
s_{02} (nm)[b]	0.77(4)	0.849(7)	0.87(3)	1.05(3)	1.03(1)	1.06(6)
s_{03} (nm)[b]	–	–	1.28(3)	1.52(9)	1.34(5)	1.60(3)
σ_1 (nm)[b]	0.037(5)	0.026(2)	0.046(6)	0.040(5)	0.06(2)	0.10(3)
σ_2 (nm)[b]	0.06(1)	0.080(7)	0.10(2)	0.15(3)	0.10(2)	0.12(4)
σ_3 (nm)[b]	–	–	0.13(6)	0.1(1)	0.16(7)	0.15(3)
w_1[b]	0.6(1)	0.40(3)	0.39(9)	0.44(6)	0.14(8)	0.4(1)
w_2[b]	0.4(1)	0.60(3)	0.39(9)	0.47(9)	0.5(1)	0.4(2)
w_3[b]	–	–	0.22(5)	0.1(2)	0.4(1)	0.22(3)

[a]Errors estimated using the blocking method. [b]Fit parameter of the $W(s)$ distribution, eq 3.

results of A3 and A4 simulations. The corresponding figure for r is reported in the Supporting Information (Figure S1). The average values of r and s, $\langle r \rangle$ and $\langle s \rangle$, respectively, indicate a more extended chain structure in A4 simulations (Table 2). The time behavior of s reveals that the PVA chain assumes different states and transitions occur between more open structures and more compact and less water exposed coils. This structural heterogeneity is more marked and present at all temperatures in A4 simulations, whereas it is triggered at the highest temperature in A3 simulations. At the aim to analyze the structural components of s behavior, we calculated the distributions of s, $W(s)$, and we fitted the $W(s)$ functions to bi- or trimodal normal distributions. In no case the $W(s)$ data could be adequately fitted with a monomodal distribution, this result showing that the chain does not exhibit a Gaussian behavior.

Figure 3 shows the results of this analysis and Table 2 reports the $W(s)$ fitting parameters at the investigated temperatures. In

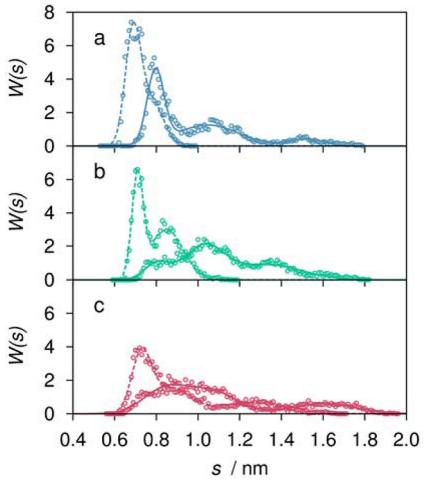

Figure 3. Distribution of values of the radius of gyration with the fitting curve of eq 3, in A4 (full line) and A3 (dashed line) simulations. T = 293 K (a), 303 K (b), and 323 K (c).

addition to the larger $\langle r \rangle$ and $\langle s \rangle$ values, the more hydrophilic character of the PVA chain in A4 simulation is supported by the presence, at all temperatures, of an extended component with radius of gyration, s_{03}, higher than 1.3 nm. In A3 simulations, the s values are smaller and display narrower distribution components, with lower σ_j and $s_{0,j}$ values. Moreover, except than at 323 K, the distributions of s in A3 simulations are bimodal, since the decreased hydrophilicity reduces the phase space of chain conformations.

A3 and A4 simulations also differ for the behavior of s as a function of temperature. In A3 simulations a monotone increase of $\langle s \rangle$ with temperature was found and a third component of s, with a larger s_0, of about 1.3 nm, was observed at the highest temperature. These findings indicate a temperature induced increase of hydrophilicity. On the contrary, in A4 simulations, the effect of temperature on s behavior is less marked and practically within errors.

The chain extension and the influence of temperature on this property are shown also by the radial distribution function between carbon atoms, $g_{C-C}(r)$ (Figure 4). The most evident

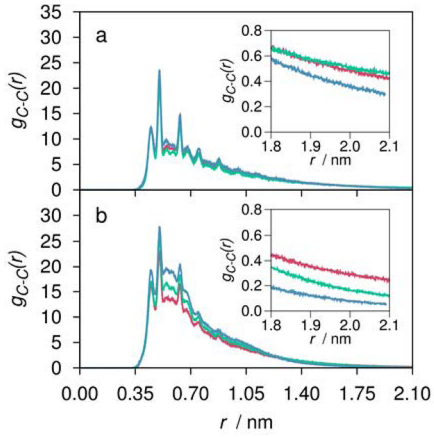

Figure 4. Radial distribution function between carbon atoms, at 293 (blue), 303 (green), and 323 K (red), in A4 (a) and A3 (b) simulations. Inset: magnification of the tail.

difference between the $g_{C-C}(r)$'s obtained in A3 and A4 simulations is the higher value of these functions in A3 simulations for distances lower than 1.4 nm. On the contrary, for distances greater than 1.4 nm the $g_{C-C}(r)$ values from A4 simulations are higher than those from A3 simulations. These characteristics prove that in A3 simulations the oligomer maintains a more compact structure. The temperature influence on the $g_{C-C}(r)$ in A3 simulations (Figure 4b) is coherent with the observed effect on s, showing an increase of chain extension with temperature.

dx.doi.org/10.1021/jp305296p | J. Phys. Chem. B 2012, 116, 10008−10019

For the comparison of these results with experimental findings, we considered both the phase behavior of PVA aqueous solutions and the temperature variation of the unperturbed chain dimension. Experimental papers reported about the complex phase behavior of PVA/water,[27,28,72] strictly related to the propensity to inter and intrachain hydrogen bonding[72,73] and characterized by metastability phenomena.[74] Choe et al.[26] observed the presence of both an upper critical solution temperature, of about 10 °C, and a lower critical solution temperature, of about 50 °C, in PVA/water solutions where the fraction of acetylated PVA residues was lower than 0.013. On the other hand, the completely deacetylated PVA was soluble in the investigated temperature and concentration intervals of 5−60 °C and 0−20% (w/w), respectively.[26] Using partial molar volume studies, it was shown that PVA bearing 20% residual acetyl groups in highly diluted aqueous solution undergoes a temperature-induced conformational change between 10 and 20 °C, with extension and/or decoiling of the chain.[75] These findings show that the aqueous solution behavior of PVA is dictated by a subtle balance of interactions, where the substitution of even a small amount of hydroxyl groups with less hydrophilic acetyl groups can heavily alter the water affinity of this macromolecule.

Concerning the effect of temperature on diluted solutions of completely deacetylated PVA, considered in this work, at our knowledge an increase of PVA water affinity at increasing temperature is not supported by available experimental data.

The temperature variation of the unperturbed chain dimension was investigated by means of thermoelasticity measurements in ethylene glycol-water mixtures on stereoregular PVA samples. A very low dependence of the unperturbed mean-square end-to-end distance, $\langle R_0^2 \rangle$, on temperature was found between 20 and 90 °C.[25] The value of $(\partial[\ln\langle R_0^2\rangle])/(\partial T)$ is negative for any tacticity, with absolute values in the order of: isotactic < atactic < syndiotactic. For an atactic PVA, with average degree of polymerization (DP) of 995 in glycol-water mixtures, the value of $(\partial[\ln\langle R_0^2\rangle])/(\partial T)$ is $(-1.2 \pm 0.1) \times 10^{-3}$ K^{-1}.[25] Nakajima and Yanagawa found the value of $(0.0 \pm 0.4) \times 10^{-3}$ K^{-1} for non stereoregular PVA, with a viscosimetric DP of 2300, in water.[76] By comparing the *r* and *s* temperature behavior obtained in our simulations with this experimental information, we can conclude that the results of A4 simulations better conform to the description obtained by experiments. Indeed the tendency of the overall chain dimension to increase at increasing temperature, observed in A3 simulations, is not in agreement to the experimental behavior of $\langle R_0^2 \rangle$, which is practically independent of temperature. Moreover the *s* trajectory at 293 K in A3 simulations, with *s* assuming values always lower than 0.8 nm (Figure 2b), reveals the presence of almost collapsed chain states, a quite unrealistic condition.

The local conformational features of the chain were explored by analyzing the distribution of values of the backbone dihedral angle, θ. For a *N*-residue linear vinyl homopolymer the $(2N - 2)$ backbone dihedrals are equivalent, therefore the distribution of conformers can be described by an unidimensional plot, shown in Figure 5 for the A3 and A4 simulations at the investigated temperatures. Accordingly with the chain atacticity, the distributions are symmetrical and the two *gauche* states, at $\theta = \pm 70°$, have equal populations. The *cis* state, at $\theta = 0°$, is practically not populated. The relative Helmholtz free energy, $A(\theta) - A(180)$, obtained as

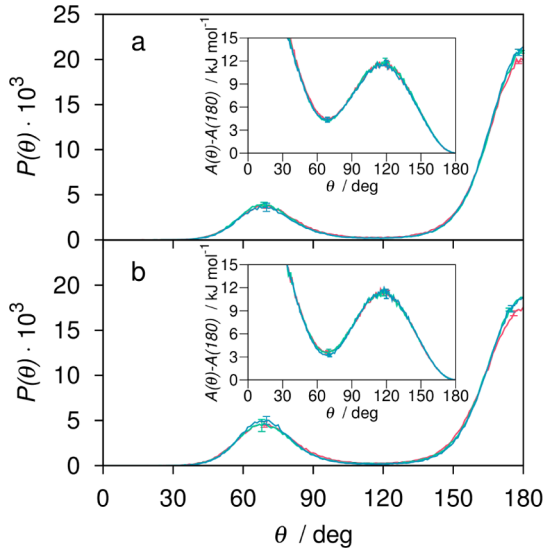

Figure 5. Backbone dihedral angles distribution in A4 (a) and A3 (b) simulations. Inset: Relative Helmholtz free energy, calculated by eq 7. T = 293 K (blue), 303 K (green), and 323 K (red).

$$A(\theta) - A(180) = -RT \ln \frac{P(\theta)}{P(180)} \tag{7}$$

where $P(\theta)$ is the distribution value and $\theta = 180°$ corresponds to the most populated *trans* conformation, is reported in the inset of Figure 5. The variation of temperature has a scarce influence on the local chain conformation, both in terms of free energy differences between equilibrium states and of free energy barriers, as shown by the almost overlapped curves of Figure 5 for the two series of simulations. According to the relation

$$\left[\frac{\partial(\Delta A)_{t-g}}{\partial T}\right]_V = -(\Delta S)_{t-g} \tag{8}$$

where $(\Delta A)_{t-g}$ and $(\Delta S)_{t-g}$ are the free energy and entropy differences between *trans* and *gauche* conformations, the negligible temperature effect on $(\Delta A)_{t-g}$ indicates that *trans* and *gauche* conformational states have very similar entropy. Therefore, the $(\Delta A)_{t-g}$ value is only dictated by the internal energy contribution, deriving from the slightly higher sterical hindrance of *gauche* states, in comparison with the sterical hindrance of *trans* conformation.

A3 and A4 simulations attain a different value for $(\Delta A)_{t-g}$, equal to 3.5 ± 0.2 and 4.4 ± 0.1 kJ/mol, respectively. The *gauche* states are therefore more favored in A3 than in A4 simulations, making easier the formation of coiled chain arrangements, as displayed by the *s* behavior in A3 simulations. The free energy barrier for the *trans*→*gauche* transition is about 11 kJ/mol for both A3 and A4 simulations. The results about the conformation distribution obtained in A4 simulations are very similar to those reported in a MD simulation study of a chemically cross-linked PVA hydrogel with high water content at 323 K.[36] The analysis of dihedral angle distribution of PVA was reported also in a MD investigation of a 15-mer in aqueous solution at 300 K.[46] For the oligomer in 5% (w/w) solution the $(\Delta A)_{t-g}$ has almost the same value obtained in A3 simulations whereas the free energy barriers between states are higher than those here reported.[46]

dx.doi.org/10.1021/jp305296p | J. Phys. Chem. B 2012, 116, 10008−10019

The fraction of backbone dihedrals in *trans* conformation, f_t, was obtained by integration of the dihedral distribution function in the range 180° ± 60°. The values of f_t are reported Table 3 and compared to the experimental value of this property, estimated by Masuda and Horii in a ^{13}C NMR CP/MASS investigation of frozen PVA aqueous solutions at 3% (w/w).[68] It is noteworthy that the large value of f_t for PVA in water is considered responsible for the formation of physical junctions in PVA hydrogels obtained by means of freezing-thawing methods.[77] Moreover the propensity of atactic PVA to form extended all-trans conformational sequences, reported by Suter and Wolf,[38] can explain the partial crystallinity of this polymer even in atactic form.[78,79] Data in Table 3 show that f_t values from A4 simulations are in better agreement with the experimental value.

Table 3. Structural and Dynamical Conformation Properties

	A3		A4	
T (K)	f_t[a]	$\langle\tau_{DIHE}\rangle$ (ps)[b]	f_t[a]	$\langle\tau_{DIHE}\rangle$ (ps)[b]
293	0.70 ± 0.02	802 ± 789	0.77 ± 0.02	613 ± 364
303	0.72 ± 0.03	398 ± 224	0.76 ± 0.01	443 ± 242
323	0.70 ± 0.01	241 ± 113	0.755 ± 0.003	271 ± 91
experimental f_t value = 0.82 at 298 K[c]				

[a]Errors estimated using the difference between the two halves of the dihedral angles distribution. [b]Average lifetime of rotational state estimated by eq 10, with root-mean-square deviation. [c]From ref 68.

The backbone dihedrals were monitored throughout the simulation to detect the transitions between rotational states. The transitions occur between the *trans* state and one of the *gauche* states, as the *cis* barrier has never been crossed during simulations. All backbone dihedral angles perform transitions, however the torsional dynamic behavior of the chain is quite heterogeneous, with some very mobile dihedral angles and other angles undergoing few transitions. This dynamic heterogeneity is more marked in A3 simulations and at the highest temperature. Moreover a higher torsional mobility was in general observed for chain-end residues, as shown by Figure S2 in the Supporting Information.

The average lifetime of rotational state, $\langle\tau_{DIHE}\rangle$, was estimated by means of eqs 9 and 10:

$$\tau_{DIHE,i} = \frac{t_{TOT}}{(N_{TRANS,i} + 1)} \quad (9)$$

$$\langle\tau_{DIHE}\rangle = \frac{1}{N_{DIHE}} \sum_{i=1}^{N_{DIHE}} \tau_{DIHE,i} \quad (10)$$

where t_{TOT}, $N_{TRANS,i}$, and N_{DIHE} are the analyzed time interval, the number of transitions of the ith dihedral angle and the number of backbone dihedral angles, respectively. The value of $\tau_{DIHE,i}$ in eq 9 corresponds to the average rotational lifetime of the ith dihedral angle and the ensemble average of this property is carried out in eq 10.

Similar $\langle\tau_{DIHE}\rangle$ values were obtained in A3 and A4 simulations (Table 3), with the exception of the lowest temperature value, where the slower chain torsional dynamics of A3 simulation is related to the more collapsed overall chain conformation, observed in the same simulation. The large errors estimated for the $\langle\tau_{DIHE}\rangle$ values in A3 simulations reflect the heterogeneity of the backbone torsional dynamics.

An investigation of PVA hydration structures and dynamic behavior in aqueous solutions, using high-frequency dielectric relaxation experiments, was recently reported by Shikata and Satokawa.[31] The authors explored a 2−8% (w/w) polymer concentration for PVA with DP of 1000 and 2000, at the temperature of 298 K. Dielectric relaxation spectra of aqueous PVA solutions were decomposed into three Debye-type relaxation modes, attributed to the rotational relaxation mode of free water molecules, to an exchange mode of PVA bound water molecules and to local motions of PVA main chains. The relaxation time corresponding to the local polymer dynamics is about 700 ps, irrespective of PVA degree of polymerization and concentration, in the 2−4% (w/w) concentration interval. This result favorably compares with the value of about 600 ps, estimated by T_1 ^{13}C NMR measurements for the relaxation time of local motions of methine and methylene groups.[31]

The local dynamics of PVA with DP about 1100 in 15% (w/w) aqueous solutions was studied as a function of temperature in a previous ^1H and ^{13}C NMR work of Zhu and Petit.[80] The authors provided an estimate of the correlation time for the backbone chain rearrangement from NMR results by applying the model of Dejean de la Batie.[81] A correlation time of 708 ps was found at 293 K and an activation energy of 30.9 kJ/mol was obtained for the local chain dynamics over a temperature range 278−360 K.[80]

The $\langle\tau_{DIHE}\rangle$ values at 293 and 303 K in A4 simulations are in reasonable agreement with the 600−700 ps experimental estimate of the characteristic time for the local chain dynamics, obtained at 298 K. It is noteworthy that no correction due to the rank is needed for the comparison of $\langle\tau_{DIHE}\rangle$ values with the relaxation time obtained in dielectric relaxation experiments, since the average lifetimes of rotational state from the MD simulations are obtained from the direct monitoring of conformational transitions.

An Arrhenius behavior is followed by A4 simulation $\langle\tau_{DIHE}\rangle$ values, giving an activation energy of 22 ± 1 kJ/mol. The difference between this value and the activation energy reported by Zhu and Petit can be ascribed to the higher concentration of PVA in the experimental study, in comparison with our simulation.

The relevance of polymer−polymer hydrogen bonding for the aqueous solution behavior of PVA is stressed in several

Table 4. Intramolecular Hydrogen Bonding[a]

	A3				A4			
T (K)	$\langle n_{HB}\rangle$[b]	$\langle n_{HB,i-(i+1)}\rangle$	$\langle\mu\rangle$	$\langle f_a\rangle$	$\langle n_{HB}\rangle$[b]	$\langle n_{HB,i-(i+1)}\rangle$	$\langle\mu\rangle$	$\langle f_a\rangle$
293	8.7(7)	8.1(7)	2.6(1)	0.44(3)	8.3(6)	7.7(4)	2.43(4)	0.44(2)
303	8.1(5)	7.5(5)	2.37(4)	0.43(3)	9.0(4)	8.4(4)	2.49(6)	0.47(2)
323	6.9(6)	6.3(4)	2.31(2)	0.37(2)	8.8(3)	8.3(2)	2.48(2)	0.47(1)
experimental $\langle f_a\rangle$ value at 298 K[c] = 0.41								

[a]Errors estimated by the blocking method. [b]Average total number of intramolecular HBs. [c]From ref 68.

dx.doi.org/10.1021/jp305296p | J. Phys. Chem. B 2012, 116, 10008−10019

experimental studies.[29,82−86] The PVA tendency to form intramolecular HBs is displayed also in dilute regime[82] and on single molecule, as reported in an atomic force microscopy investigation.[29] We analyzed the trajectory for the occurrence of this interaction both between near-neighboring residues (forming intradyad HBs) and between topologically more distant PVA residues. The values of average number of intramolecular HBs *per* PVA residue, reported in Table 4, show that practically only intradyad HBs occur in the 30-mer. A similar result was found by Müller Plathe in MD simulation of a 15-mer in water.[46] However, the absence of intramolecular HBs between nonadjacent residues is in contrast with some experimental findings obtained on PVA solutions. Indeed, intramolecular HBs were found to affect the chain conformation[83,84] and to govern the elastic properties[29] of PVA with DPs of few thousands. Such a behavior leads to conclude that part of these HBs involves nonadjacent residues. Therefore, the lack of intramolecular HBs between distant residues, observed in the 30-mer simulations, suggests that the intramolecular PVA connectivity can be established between chain domains separated by more than 30 residues.

The insets of Figures 6 (A4 results) and 7 (A3 results) show the autocorrelation function of intramolecular HBs, that, as

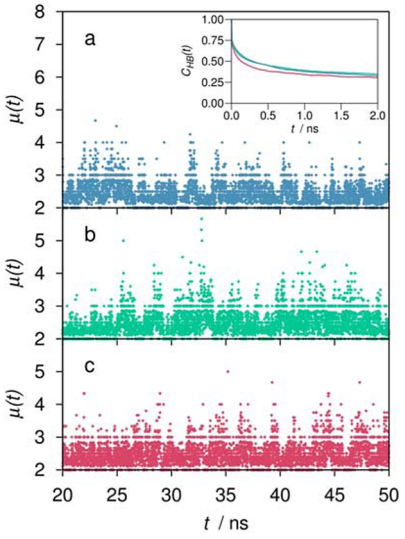

Figure 6. Trajectory of the average length (in residues) of sequences connected by intradyad HBs in A4 simulations. Inset: Decay of the HB autocorrelation function between PVA hydroxyl groups. T = 293 K (blue), 303 K (green), and 323 K (red).

expected, does not completely decay for the continue formation/break of these HBs. The average fraction of PVA residues involved in intradyad HB, $\langle f_a \rangle$, was calculated by means of eq 4, as described in section 2. To obtain the $\langle f_a \rangle$ value, we analyzed the trajectory searching for sequences of adjacent residues mutually connected by HB (Figure 1). The average number of residues composing these sequences, reported in Table 4, is between 2 and 3, although trajectory frames with HB connected sequences of 5 or 6 residues were observed, as shown in Figures 6 and 7. Table 4 reports $\langle f_a \rangle$ as a function of temperature, in comparison with the experimental value of this property, obtained for PVA with DP of 1700 in 3% (w/w) aqueous solution by means of CP/MAS ^{13}C NMR measurements.[68] In A4 simulations $\langle f_a \rangle$ is scarcely dependent on temperature, whereas in A3 simulations a decreasing trend

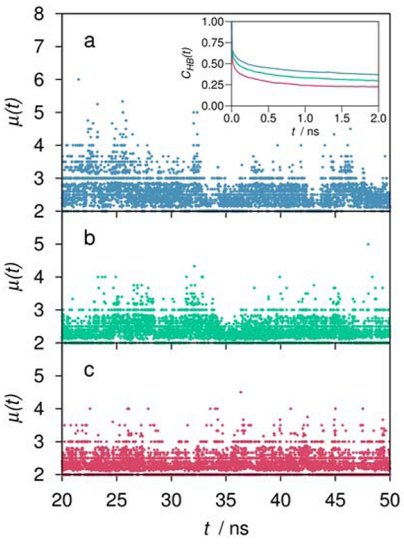

Figure 7. Trajectory of the average length (in residues) of sequences connected by intradyad HBs in A3 simulations. Inset: Decay of the HB autocorrelation function between PVA hydroxyl groups. T = 293 K (blue), 303 K (green), and 323 K (red).

with temperature can be noted. Both A3 and A4 simulations overestimate of about 10% the $\langle f_a \rangle$ value, a result in satisfactory agreement with the experimental value.

3.2. PVA−Water Interaction. The polymer induced modification of water properties in PVA hydrogels and solutions was investigated by means of different experimental methods.[31−33,87] The common picture emerging from these studies is a slowing effect on water dynamics, however some uncertainty remains on the amount of solvent affected by PVA interaction, in particular in highly diluted solutions. A hydration number per residue of about 2 was estimated by high-frequency dielectric relaxation measurements on 2−8% (w/w) PVA aqueous solutions at 25 °C.[31] Differential scanning calorimetry (DSC) experiments were used to measure the amount of non freezable water in PVA solutions. This solvent component is considered strongly interacting with polymer. With such experiments the presence of no more than 2 coordinated water molecules per residue was confirmed in 10% (w/w) PVA solutions.[33] However, Cheng et al.,[32] using the same DSC approach, reported an increasing hydration number of PVA with the decrease of concentration, up to a maximum value of about 7 water molecules per residue in 1−2% (w/w) PVA solutions. Moreover the DSC result for the 1% (w/w) PVA solution, reported in Figure 6 of ref 33, corresponds to 4.5 coordinating water molecules per residue. Therefore, an increase of the influence sphere of PVA over surrounding water occurs in the dilute regime.

MD simulations can properly elucidate these experimental findings on a molecular basis. In this respect our simulations, modeling a solution with the lowest concentration of hitherto reported MD simulation works on PVA, is adequate to explain the hydration features of this polymer in dilute solution. The analysis of properties related to solvent interaction, having a time scale of few picoseconds, was carried out on three frequently sampled portions of trajectory, selected along the 30 ns production run, as described in section 2. The figure showing the analyzed time intervals along the radius of gyration trajectory is reported in the Supporting Information (Figure S3). With this procedure we sampled the system in different

dx.doi.org/10.1021/jp305296p | J. Phys. Chem. B 2012, 116, 10008−10019

chain states, in order to account for the oligomer structural heterogeneity.

Figure 8 shows the radial distribution function between PVA and water oxygen atoms, $g_{O\text{-}OW}(r)$, as a function of temperature.

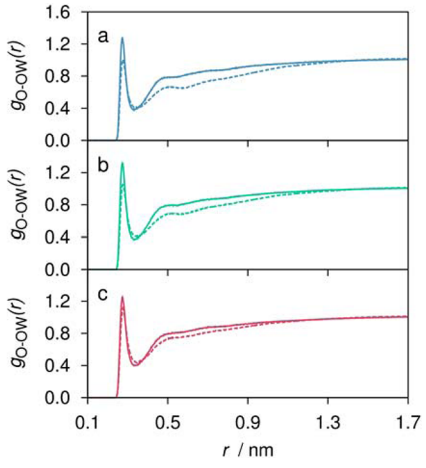

Figure 8. Radial distribution function between PVA and water oxygen atoms in A4 (full line) and A3 (dashed line) simulations. T = 293 K (a), 303 K (b), and 323 K (c).

The $g_{O\text{-}OW}(r)$ profile displays the PVA structuring effect on the surrounding water, extending to a maximum distance from the polymer of about 1.2 nm. The first minimum distance of the $g_{O\text{-}OW}(r)$, at about 0.33 and 0.35 nm in A4 and A3 simulations, respectively, indicates the thickness of the first PVA hydration shell. The second hydration shell, corresponding to the less marked second minimum of the $g_{O\text{-}OW}(r)$, has a thickness of about 0.55 and 0.57 nm in A4 and A3 simulations, respectively. From Figure 8 it can be noted that the water ordering around PVA hydroxyl groups is lower in A3 than in A4 simulations. This result is in agreement with the lower exposition to the solvent of the chain found in A3 simulations. The water oxygen coordination number of PVA oxygen atoms, $n_{O\text{-}OW}$, obtained by integration of the $g_{O\text{-}OW}(r)$, is reported in Table 5. A value of about 2 is obtained for $n_{O\text{-}OW}$ in both simulations, with an increasing trend with temperature in A3 simulations. The average number of water molecules per PVA residue residing within the second hydration shell for at least 10 ps, $n_{W,shell}$, was calculated by direct analysis of trajectory. As shown in Table 5, the $n_{W,shell}$ values in A3 simulations are lower than in A4 simulations, a finding coherent with the more collapsed chain state.

The results of the analysis of hydrogen bonding between PVA and water are reported in Table 5, showing the average number of HBs per residue, $n_{HB,inter}$, and the average lifetime of this interaction, $\tau_{HB,inter}$, obtained as described in section 2. The $\tau_{HB,inter}$ values are always higher than the average lifetimes of HBs formed between water molecules ($\tau_{HB,w}$ values in Table 6). This result was expectable since, using the intermittent HB autocorrelation function, the HB lifetime is affected by the diffusion dynamics of both donor and acceptor groups. The diffusion coefficient of the segmental motions of PVA chain, estimated by quasi-elastic neutron scattering measurements, is about $^1/_4$ the water diffusion coefficient.[37] Therefore, the higher value of the average lifetime of PVA-water HBs, compared to the average lifetime of water−water HBs, is a consequence of the slower diffusion dynamics of PVA, in comparison to the diffusivity of water molecules.

For A4 simulations the dependence of $n_{HB,inter}$ values on temperature is within errors, confirming that the structural characteristics of the solvation are scarcely affected by temperature. On the contrary, in A3 simulations $n_{HB,inter}$ has an increasing trend with temperature.

The analysis of $g_{O\text{-}OW}(r)$ and intermolecular hydrogen bonding reveals that the polymer−water interaction is stronger in A4 than in A3 simulations, as indicated by the higher values of coordination number and $n_{HB,inter}$. The structural differences in the solvation cause a dynamical difference, with longer lifetimes of the polymer−water hydrogen bonds in A4 than in A3 simulations (see $\tau_{HB,inter}$ values in Table 5).

These solvation features support a lower hydrophilicity of PVA in A3 than in A4 simulations, found in the overall chain behavior analysis. The correlation between the temperature effects on the hydration features and on the radius of gyration proves the synergy between solvent interaction and chain behavior.

The $\tau_{HB,inter}$ values at 293 and 303 K can be compared with the relaxation time attributed to an exchange mode of PVA bound water molecules in 3% (w/w) solution of PVA with DP 1000 at 298 K, in the previously cited high-frequency dielectric relaxation study of Shikata and Satokawa.[31] The authors find a relaxation time of 27 ps for the exchange mode of PVA hydrating water and a relaxation time of about 8 ps for the rotational relaxation mode of free water in the solution. The $\tau_{HB,inter}$ values from A4 simulations are in better agreement with the experimental relaxation time, although the computed values are about half the experimental one. This discrepancy can be considered acceptable, taking into account the semiquantitative character of the comparison between time constants related to intermolecular HB dynamics and dipolar relaxation. However it is noteworthy that the simulation effectively reproduces the extent of the polymer influence on water mobility. Indeed the ratio between the experimental times of 27 and 8 ps,[31] equal to about 3.4, corresponds, within errors, to the ratio between the $\tau_{HB,inter}$ value (Table 5) and the lifetime of HB between water

Table 5. PVA Hydration Features

	A3				A4			
T (K)	$n_{O\text{-}OW}$ [a,b]	$n_{W,shell}$ [b,c] (per PVA residue)	$n_{HB,inter}$ [d] (per PVA residue)	$\tau_{HB,inter}$ [b] (ps)	$n_{O\text{-}OW}$ [a,b]	$n_{W,shell}$ [b,c] (per PVA residue)	$n_{HB,inter}$ [d] (per PVA residue)	$\tau_{HB,inter}$ [b] (ps)
293	1.9(1)	5.2(3)	1.22(3)	10(1)	1.9(2)	6.8(3)	1.48(1)	13(3)
303	2.0(2)	5.3(2)	1.29(1)	8.3(5)	1.9(1)	6.5(3)	1.54(3)	11(2)
323	2.1(2)	5.5(3)	1.38(1)	6(1)	1.9(1)	6.0(3)	1.50(5)	7(1)

[a]Coordination number, estimated by integration of $g_{O\text{-}OW}(r)$. [b]Errors estimated using the standard deviation of the data sets from the three frequently sampled trajectory intervals. [c]Number of water molecules staying within the second PVA hydration shell for at least 10 ps. [d]Errors estimated using the blocking method.

dx.doi.org/10.1021/jp305296p | J. Phys. Chem. B 2012, 116, 10008−10019

Table 6. Water Properties[a]

	A3						A4							
	A domain			B domain			A domain			B domain			bulk water	
T (K)	$n_{HB,w}$[b]	$\tau_{HB,w}$[c] (ps)	$D_w/D_{w,bulk}$	$n_{HB,w}$[b]	$\tau_{HB,w}$[c] (ps)	$D_w/D_{w,bulk}$	$n_{HB,w}$[b]	$\tau_{HB,w}$[c] (ps)	$D_w/D_{w,bulk}$	$n_{HB,w}$[b]	$\tau_{HB,w}$[c] (ps)	$D_w/D_{w,bulk}$	$n_{HB,w}$[b]	$\tau_{HB,w}$[c,d] (ps)
293	1.54(8)	7.1(2)	0.6(2)	1.42(3)	3.31(7)	1.0(1)	1.54(6)	7.6(4)	0.6(1)	1.41(4)	3.4(1)	1.0(1)	1.45(2)	3.30(8)
303	1.51(8)	5.7(2)	0.6(1)	1.40(4)	2.82(5)	1.0(1)	1.52(8)	6.1(2)	0.6(1)	1.36(6)	2.78(3)	1.0(1)	1.41(1)	2.54(4)
323	1.46(7)	3.9(1)	0.6(1)	1.33(4)	2.06(5)	0.9(1)	1.46(8)	4.1(1)	0.6(1)	1.31(6)	2.02(4)	0.9(1)	1.37(1)	1.97(4)

[a]Errors estimated using the standard deviation of the data sets obtained by dividing each frequently sampled trajectory into 49 intervals of 10 ps. [b]Average number of HBs per water molecule. The value of $n_{HB,w}$ multiplied by 2 corresponds to the average hydration number of water molecules. [c]Average lifetime of HB between water molecules. Error estimated using the standard deviation of the data sets from the three frequently sampled trajectory intervals. [d]Errors estimated using the same relative errors as those of the $\tau_{HB,w}$'s obtained for the B domains.

molecules in a domain far from the polymer ($\tau_{HB,w}$ value of B domain in Table 6).

The average number of HBs per PVA residue is in satisfactory agreement with the value of 2.2, estimated as PVA hydration number in dilute solution by dielectric relaxation measurements.[31] In addition, the comparison between $n_{O\text{-}OW}$ and $n_{HB,inter}$ values in Table 5 shows that the water molecules of the first coordination shell of PVA hydroxyl groups are largely involved in HB with the polymer.

By assuming that the structural organization of water in the vicinity of PVA hydroxyl groups is not significantly altered by a moderate temperature variation, we can use the simulation results about the polymer hydration features to interpret the experimental data of nonfreezable water. This assumption is supported by the results of quasi-elastic neutron scattering experiments on PVA hydrogels at high hydration degree, showing that the amount of supercooled water is independent of temperature in the interval 291−323 K.[87] Accordingly, in A4 simulations we observe that $n_{HB,inter}$ and $n_{O\text{-}OW}$ values are unchanged at 293, 313, and 323 K (Table 5).

DSC experiments on PVA dilute solutions found a number of nonfreezable water molecules per PVA residue equal to 5−7,[32] therefore the nonfreezable solvent belongs not only to the first but also to the second PVA hydration shell. The comparison of the last experimental value with $n_{W,shell}$ values in Table 5 identifies the not-freezing water component with the solvent molecules residing within the second hydration shell. Such an effect denotes a polymer influence both on structural and dynamical properties of water, deeply investigated in the trajectory analysis.

For this analysis water molecules were separated in two domains. Solvent molecules belonging to the first and second hydration shell of PVA were included in domain A, the remaining water forming domain B. Domain A accounts for about 8% of total water in solution. The effect of polymer interaction on water structure was explored by investigating the number of HBs formed by solvent molecules in both domains. Data in Table 6 indicate an increase of hydrogen bonding for water in domain A, whereas water in domain B behaves similarly to bulk water. The analysis of the time decay of the autocorrelation function of HB between water molecules highlights a slowing effect on water dynamics in domain A, measured by values of the lifetime of HB between water molecules, $\tau_{HB,w}$, in Table 6. The same effect is showed by the value of the ratio between the diffusion coefficient of water molecules staying within the second hydration shell and the diffusion coefficient of bulk water, $D_w/D_{w,bulk}$, reported in Table 6. It is noteworthy the sensible quenching of the dynamics of water residing in these surroundings of PVA. Such supercooled and superstructured water component cannot participate to the solvent freezing process, as observed in DSC experiments on PVA solutions.[32]

The description of the solvent behavior obtained in these simulations provides a molecular interpretation of recently reported results on macro- and microscale rheological properties of PVA aqueous solutions.[33] In this experimental study, Milosavljevic et al. concluded that PVA aqueous solutions can be envisioned as dynamic systems comprising hydrated PVA molecules and "interconnected water pools" (located between macromolecules), the rheological properties of which are very similar to that of pure water. Fluorescence depolarization measurements indicated that pool sizes are relatively large, which was corroborated by DSC measurements that showed that each PVA hydroxyl group interacts with no more than two water molecules.[33] These findings and our simulation results reciprocally support the picture of PVA diluted solution as a compartmentalized environment, with unperturbed water domains and regions containing water structurally and dynamically coupled with the polymer.

Concerning the comparison between A3 and A4 simulations, the differences between values of water properties in solution (Table 6) are within errors, a not surprising result taking into account the kind of difference between the two protocols.

4. CONCLUDING REMARKS

The modification of PVA partial charges according to the G45A4 GROMACS force field improves the MD simulation modeling of PVA aqueous solution, in comparison to simulation with G45A3 GROMACS force field. The main difference between results of the two protocols concerns the nature of interaction with water, leading A4 simulations to a better description of the hydrophilicity of PVA and of the temperature effect on the chain dimension. The agreement of A4 simulation findings with available experimental data, concerning conformation features, intramolecular hydrogen bonding, local polymer dynamics and hydration is almost quantitative.

New structural characteristics of PVA are highlighted in this study. A heterogeneity of overall chain states, coupled with a different solvent interaction, emerges in the explored time-window. The absence of hydrogen bonds between nonadjacent PVA residues suggests that HB stabilized intrachain entanglements can be formed only in segments with more than 30 residues. This result has implications in the estimate of the mesh size in chemically cross-linked PVA hydrogels, where the network porosity can be affected by physical junctions in addition to chemical cross-links.

The sphere of influence of PVA on water includes about six water molecules per residue, which are perturbed both structurally, with an increase of hydrogen bonding, and dynamically, with almost a halving and doubling of diffusion coefficient and residence time, respectively. This characteristic, supported by a corresponding experimental datum,[32] is relevant for applications where PVA is implicated as soft biomaterial or as component of biosensing devices,[88−90] since possible unwanted interactions of biological compounds with the polymer can be screened by a kinetically stable water shell.

The present study is also meant as a test of a MD simulation protocol for PVA-based systems in aqueous environment. In this respect, it provides the elements for evaluating the potentialities and the limits of classical MD simulation in the investigation of such systems.

■ ASSOCIATED CONTENT

Supporting Information

Figure S1, trajectory of the end to end distance; Figure S2, single dihedral torsional mobility; and Figure S3, radius of gyration trajectory with the time intervals used for PVA−water interaction analysis. This material is available free of charge via the Internet at http://pubs.acs.org.

■ AUTHOR INFORMATION

Corresponding Author

*E-mail: ester.chiessi@uniroma2.it.

Notes

The authors declare no competing financial interest.

■ ACKNOWLEDGMENTS

We thank the CINECA Supercomputing Centre for supplying the computing resources of this investigation. The simulation work was performed within the CINECA ISCRA project FALSTAFF (2011).

■ REFERENCES

(1) Herrmann, W. O.; Heahnel, W. German Patent 450.286, 1924.
(2) Ahn, S.-M.; Ha, J.-W.; Kim, J.-H.; Lee, Y.-T.; Lee, S.-B. *J. Membr. Sci.* **2005**, *247*, 51.
(3) Peters, T. A.; Poeth, C. H. S.; Benes, N. E.; Buijs, H. C. W. M.; Vercauteren, F. F.; Keurentjes, J. T. F. *J. Membr. Sci.* **2006**, *276*, 42.
(4) Zhang, Q. G.; Liu, Q. L.; Zhu, A. M.; Xiong, Y.; Ren, L. *J. Membr. Sci.* **2009**, *335*, 68.
(5) Choi, J. H.; Jegal, J.; Kim, W. N.; Choi, H. S. *J. Appl. Polym. Sci.* **2009**, *111*, 2186.
(6) Chuangchote, S.; Supaphol, P. *J. Nanosci. Nanotechnol.* **2006**, *6*, 125.
(7) López-Rubio, A.; Sanchez, E.; Sanz, Y.; Lagaron, J. M. *Biomacromolecules* **2009**, *10*, 2823.
(8) Chiellini, E.; Corti, A.; Antone, S. D.; Solaro, R. *Prog. Polym. Sci.* **2003**, *28*, 963.
(9) Kawai, F.; Hu, X. *Appl. Microbiol. Biotechnol.* **2009**, *84*, 227.
(10) Chiellini, E.; Corti, A.; Del Sarto, G.; D'Antone, S. *Polym. Degrad. Stab.* **2006**, *91*, 3397.
(11) Lindemann, M. K. In *Encyclopedia of Polymer Science and Engineering*; Mark, H. F., Gaylord, N. G., Eds.; Wiley-Interscience: New York, 1971; Vol. *14*, p 149.
(12) Kaneo, Y.; Hashihama, S.; Kakinoki, A.; Tanaka, T.; Nakano, T.; Ikeda, Y. *Drug Metab. Pharmacokinet.* **2005**, *20*, 435.
(13) Juntanon, K.; Niamlang, S.; Rujiravanit, R.; Sirivat, A. *Int. J. Pharm.* **2008**, *356*, 1.
(14) Mawad, D.; Poole-Warren, L. A.; Martens, P.; H. Koole, L. H.; Slots, T. L. B.; van Hooy-Corstjens, C. S. J. *Biomacromolecules* **2008**, *9*, 263.
(15) Cavalieri, F.; Chiessi, E.; Villa, R.; Viganò, L.; Zaffaroni, N.; Telling, M. F.; Paradossi, G. *Biomacromolecules* **2008**, *9*, 1967.
(16) Ghugare, S. V.; Mozetic, P.; Paradossi, G. *Biomacromolecules* **2009**, *10*, 1589.
(17) Alves, M.-H.; Jensen, B. E. B.; Smith, A. A. A.; Zelikin, A. N. *Macromol. Biosci.* **2011**, *11*, 1293.
(18) Cavalieri, F.; Finelli, I.; Tortora, M.; Mozetic, P.; Chiessi, E.; Polizio, F.; Brismar, T. B.; Paradossi, G. *Chem. Mater.* **2008**, *20*, 3254.
(19) Galbiati, A.; Tabolacci, C.; Morozzo Della Rocca, B.; Beninati, S.; Desideri, A.; Paradossi, G. *Mater. Sci. Eng.: C* **2011**, *31*, 1653.
(20) Sciallero, C.; Paradossi, G.; Trucco, A. *Ultrasonics* **2012**, *52*, 456.
(21) Hassan, C. M.; Peppas, N. A. *Adv. Polym. Sci.* **2000**, *153*, 37.
(22) Lozinsky, V. I. *Russ. Chem. Rev.* **1998**, *67*, 573. Lozinsky, V. I.; Galaev, I. Y.; Plieva, F. M.; Savina, I. N.; Jungvid, H.; Mattiasson, B. *Trends Biotechnol.* **2003**, *21*, 445.
(23) Peppas, N. M. *Makromol. Chem.* **1975**, *176*, 3433. Stauffer, S.; Peppas, N. A. *Polymer* **1992**, *33*, 3932.
(24) Lozinsky, V. I.; Damshkaln, L. G. *J. Appl. Polym. Sci.* **2000**, *77*, 2017.
(25) Sakurada, I.; Nakajima, A.; Shibatani, K. *Makromol. Chem.* **1965**, *87*, 103.
(26) Pae, B. J.; Moon, T. J.; Lee, C. H.; Ko, M. B.; Park, M.; Lim, S.; Kim, J.; Choe, C. R. *Korea Polym. J.* **1997**, *5*, 126.
(27) Zubov, P. I.; Osipov, Y. A.; Sukhareva, L. A. *Vysokomol. Soyed.* **1964**, *6*, 811.
(28) Klenina, O. V.; Klenin, V. I.; Frenkel, S. Y. *Vysokomol. Soyed.* **1970**, *A12*, 1277.
(29) Li, H.; Zhang, W.; Xu, W.; Zhang, X. *Macromolecules* **2000**, *33*, 465.
(30) Komatsu, M.; Inoue, T.; Miyasaka, K. *J. Polym. Sci., B: Polym. Phys.* **1986**, *24*, 303.
(31) Satokawa, Y.; Shikata, T. *Macromolecules* **2008**, *41*, 2908.
(32) Li, W.; Zheng, Y.; Cheng, R. *Polymer* **2008**, *49*, 4740.
(33) Krise, K. M.; Hwang, A. A.; Sovic, D. M.; Milosavljevic, B. H. *J. Phys. Chem B* **2011**, *115*, 2759.
(34) Chiessi, E.; Lonardi, A.; Paradossi, G. *J. Phys. Chem. B* **2010**, *114*, 8301.
(35) Chiessi, E.; Autieri, E.; Lonardi, A.; Paradossi, G.; Sega, M. *J. Phys. Chem. B* **2011**, *115*, 5827.
(36) Chiessi, E.; Cavalieri, F.; Paradossi, G. *J. Phys. Chem. B* **2007**, *111*, 2820.
(37) Paradossi, G.; Finelli, I.; Natali, F.; Telling, M. T. F.; Chiessi, E. *Polymers* **2011**, *3*, 1805.
(38) Wolf, R. M.; Suter, U. W. *Macromolecules* **1984**, *17*, 669.
(39) Tamai, Y.; Tanaka, H.; Nakanishi, K. *Mol. Simul.* **1996**, *16*, 359.
(40) Tamai, Y.; Tanaka, H.; Nakanishi, K. *Macromolecules* **1996**, *29*, 6750.
(41) Tamai, Y.; Tanaka, H.; Nakanishi, K. *Macromolecules* **1996**, *29*, 6761.
(42) Tamai, Y.; Tanaka, H. *Chem. Phys. Lett.* **1998**, *285*, 127.
(43) Tamai, Y.; Tanaka, H. *Fluid Phase Equilib.* **1998**, *144*, 441.
(44) Tamai, Y.; Tanaka, H. *Phys. Rev. E* **1999**, *59*, 5647.
(45) Tamai, Y.; Tanaka, H. *Mol. Simul.* **1999**, *21*, 283.
(46) Müller-Plathe, F.; van Gunsteren, W. F. *Polymer* **1997**, *38*, 2259.
(47) Müller-Plathe, F. *Macromolecules* **1998**, *31*, 6721.
(48) Müller-Plathe, F. *J. Membr. Sci.* **1998**, *141*, 147.
(49) Karlsson, G. E.; Johansson, T. S.; Gedde, U. W.; Hedenqvist, M. S. *J. Macromol. Sci. Part B* **2002**, *42*, 185.
(50) Karlsson, G. E.; Gedde, U. W.; Hedenqvist, M. S. *Polymer* **2004**, *45*, 3893.
(51) Bermejo, J. S.; Ugarte, C. M. *J. Chem. Phys.* **2008**, *129*, 154907.
(52) Wu, C. *Polymer* **2010**, *51*, 4452.
(53) Bryk, T.; Holovko, M. *J. Mol. Liq.* **2009**, *147*, 13.
(54) Berendsen, H. J. C.; van der Spoel, D.; van Drunen, R. *Comput. Phys. Commun.* **1995**, *91*, 43.
(55) Lindahl, E.; Hess, B.; van der Spoel, D. *J. Mol. Model.* **2001**, *7*, 306.
(56) van der Spoel, D.; Lindahl, E.; Hess, B.; Groenhof, G.; Mark, A. E.; Berendsen, H. J. C. *J. Comput. Chem.* **2005**, *26*, 1701.

(57) Schuler, L. D.; van Gunsteren, W. F. *Mol. Simul.* **2000**, *25*, 301.
(58) Schuler, L. D.; Daura, X.; van Gunsteren, W. F. *J. Comput. Chem.* **2001**, *22*, 1205.
(59) Lins, R. D.; Hünenberger, P. H. *J. Comput. Chem.* **2005**, *26*, 1400.
(60) Berendsen, H. J. C.; Postma, J. P. M.; van Gunsteren, W. F.; Hermans, J. In *Intermolecular Forces*; Pullman, B., Ed.; Reidel: Dordrecht, The Netherlands, 1981; p 239.
(61) Brooks, B. R.; Brooks, C. L., 3rd; Mackerell, A. D., Jr; Nilsson, L.; Petrella, R. J.; Roux, B.; Won, Y.; Archontis, G.; Bartels, C.; Boresch, S.; Caflisch, A.; Caves, L.; Cui, Q.; Dinner, A. R.; Feig, M.; Fischer, S.; Gao, J.; Hodoscek, M.; Im, W.; Kuczera, K.; Lazaridis, T.; Ma, J.; Ovchinnikov, V.; Paci, E.; Pastor, R. W.; Post, C. B.; Pu, J. Z.; Schaefer, M.; Tidor, B.; Venable, R. M.; Woodcock, H. L.; Wu, X.; Yang, W.; York, D. M.; Karplus, M. *J. Comput. Chem.* **2009**, *30*, 1545.
(62) Kurata, M.; Tsunashima, Y. *Polymer Handbook*, 4th ed.; Brandrup, J., Immergut, E. H., Grulke, E. A.; Eds.; John Wiley & Sons: New York, 1999; Vol. *VII*, p 53.
(63) Hockney, R. W. *Methods Comput. Phys.* **1970**, *9*, 136.
(64) Hess, B.; Bekker, H.; Berendsen, H. J. C.; Fraaije, J. G. E. M. *J. Comput. Chem.* **1997**, *18*, 1463.
(65) Berendsen, H. J. C.; Postma, J. P. M.; van Gunsteren, W. F.; Di Nola, A.; Haak, J. R. *J. Chem. Phys.* **1984**, *81*, 3684.
(66) Essmann, U.; Perera, L.; Berkowitz, M. L.; Darden, T.; Lee, H.; Pedersen, L. G. *J. Chem. Phys.* **1995**, *103*, 8577.
(67) Bussi, G.; Donadio, D.; Parrinello, M. *J. Chem. Phys.* **2007**, *126*, 014101.
(68) Masuda, K.; Horii, F. *Macromolecules* **1998**, *31*, 5810.
(69) Rapaport, D. C. *Mol. Phys.* **1983**, *50*, 1151.
(70) Luzar, A. *J. Chem. Phys.* **2000**, *113*, 10663.
(71) Humphrey, W.; Dalke, A.; Schulten, K. *J. Mol. Graphics* **1996**, *14*, 33.
(72) Borchard, W. In *Chemistry and Technology of Water-Soluble Polymers*; Finch, C. A., Ed.; Plenum Press: New York, 1983; p 113−124.
(73) Briscoe, B.; Luckham, P.; Zhu, S. *Polymer* **2000**, *41*, 3851.
(74) Klenin, V. I.; Klenina, O. V.; Kolchanov, V. A.; Shvartsburd, B. I.; Frenkel, S. Y. *Polym. Sci. U.S.S.R.* **1974**, *16*, 2731.
(75) Crowther, N. J.; Eagland, D. *J. Chem. Soc., Faraday Trans. 1* **1986**, *82*, 2791.
(76) Nakajima, A.; Yanagawa, H. *J. Phys. Chem.* **1963**, *67*, 654.
(77) Peppas, H. *Adv. Polym. Sci.* **2000**, *153*, 37.
(78) Masuda, K.; Kaji, H.; Horii, F. *J. Polym. Sci., Part B: Polym. Phys.* **2000**, *38*, 1.
(79) Beresniewicz, A. *J. Polym. Sci.* **1959**, *35*, 497.
(80) Zhu, X. X.; Petit, J.-M. *Macromolecules* **1996**, *29*, 2075.
(81) Dejean de la Batie, R.; Lauprêtre, F.; Monnerie, L. *Macromolecules* **1988**, *21*, 2045.
(82) Liu, M.; Cheng, R.; Wu, C.; Qian, R. *J. Polym. Sci., Part B: Polym. Phys.* **1997**, *35*, 2421.
(83) Takigawa, T.; Urayama, K.; Masuda, T. *Chem. Phys. Lett.* **1990**, *174*, 259.
(84) Takigawa, T.; Urayama, K.; Masuda, T. *J. Chem. Phys.* **1990**, *93*, 7310.
(85) Yang, H.; Cheng, R.; Xie, H.; Wang, Z. *Polymer* **2005**, *46*, 7557.
(86) Finch, C. A., Ed. *Polyvinyl Alcohols Developments*; JohnWiley & Sons: Chichester, U.K., 1992.
(87) Paradossi, G.; Cavalieri, F.; Chiessi, E.; Telling, M. T. F. *J. Phys. Chem. B* **2003**, *107*, 8363.
(88) Studentsov, Y. Y.; Schiffman, M.; Strickler, H. D.; Ho, G. Y. F.; Pang, Y.-Y. S.; Schiller, J.; Herrero, R.; Burk, R. D. *J. Clin. Microbiol.* **2002**, *40*, 1755.
(89) Omidfar, K.; Zarei, H.; Gholizadeh, F.; Larijani, B. *Anal. Biochem.* **2012**, *421*, 649.
(90) Omidfar, K.; Dehdast, A.; Zarei, H.; Sourkohi, B. K.; Larijani, B. *Biosens. Bioelectron.* **2011**, *26*, 4177.